Possible coupling between magnons and phonons in multiferroic $CaMn_7O_{12}$

Filip Kadlec,[1,*] Veronica Goian,[1] Christelle Kadlec,[1] Martin Kempa,[1] Přemysl Vaněk,[1] Jon Taylor,[2] Stéphane Rols,[3] Jan Prokleška,[4] Milan Orlita,[5] and Stanislav Kamba[1,*]

[1]*Institute of Physics, Academy of Sciences of the Czech Republic, Na Slovance 2, 182 21 Prague 8, Czech Republic*

[2]*ISIS Facility, Rutherford Appleton Laboratory, Chilton, Didcot, United Kingdom*

[3]*Institut Laue-Langevin, Boîte Postale 156, 38042 Grenoble Cedex 9, France*

[4]*Department of Condensed Matter Physics, Faculty of Mathematics and Physics, Charles University, Ke Karlovu 5, 121 16 Prague 2, Czech Republic*

[5]*Grenoble High Magnetic Field Laboratory, CNRS, 25, avenue des Martyrs, Grenoble Cedex 9, France*

(Received 17 April 2014; revised manuscript received 7 August 2014; published 28 August 2014)

Spin and lattice dynamics of $CaMn_7O_{12}$ ceramics were investigated using infrared, THz, and inelastic neutron scattering (INS) spectroscopies in the temperature range 2 to 590 K, and, at low temperatures, in applied magnetic fields of up to 12 T. On cooling, we observed phonon splitting accompanying the structural phase transition at $T_C = 450$ K as well as the onset of the incommensurately modulated structure at 250 K. In the two antiferromagnetic phases below $T_{N1} = 90$ K and $T_{N2} = 48$ K, several infrared-active excitations emerge in the meV range; their frequencies correspond to the maxima in the magnon density of states obtained by INS. At the magnetic phase transitions, these modes display strong anomalies and, for some of them, a transfer of dielectric strength from the higher-frequency phonons is observed. We propose that these modes are electromagnons. Remarkably, at least two of these modes remain active also in the paramagnetic phase; for this reason, we call them paraelectromagnons. In accordance with this observation, quasielastic neutron scattering revealed short-range magnetic correlations persisting within temperatures up to 500 K above T_{N1}.

DOI: 10.1103/PhysRevB.90.054307 PACS number(s): 75.85.+t, 75.30.Ds, 63.20.kk, 78.20.Ci

I. INTRODUCTION

Electromagnons are collective spin excitations occurring in many magnetoelectric multiferroics, contributing to their dielectric response and potentially also to the magnetic one [1–4]. They appear especially in the THz-range spectra below phonons, and they are frequently understood as spin waves excited by the electric component of the incident electromagnetic radiation; more precisely, they contribute to the off-diagonal components of the magnetoelectric susceptibility tensor. Although electromagnons were observed in a variety of multiferroics, there is still no universal microscopic theory which would explain the mechanisms giving rise to electromagnons. Depending on the crystalline and magnetic structure, the magnons can be activated in the THz-range dielectric spectra by one of the following magnetoelectric coupling mechanisms: the magnetostriction [5,6], inverse Dzyaloshinskii-Moriya interaction [7,8], or spin-dependent hybridization of the p and d orbitals [9]. Interestingly, in one material, the magnetoelectric coupling mechanism leading to activation of electromagnons can be different from the one giving rise to the static spin-induced polarization. For example, in the well-known multiferroic $TbMnO_3$, the polarization is induced by the inverse Dzyaloshinskii-Moriya mechanism, while at least some electromagnons are activated by magnetostriction [5]. Furthermore, it is still unclear how the electromagnons exhibiting a wave vector off the Brillouin-zone (BZ) center can be excited by the incident photons with wave vectors near the BZ center, $q \approx 0$; it seems that this may be allowed by the modulation of the magnetic structure. Generally speaking, the electromagnons as excitations which are both electric- and magnetic-dipole active reveal the dynamical features of the magnetoelectric coupling [5–9], and studying their temperature- and magnetic-field-dependent properties may provide insight into the symmetry of the spin subsystem of the materials.

Among the many spin-driven multiferroics which have been studied intensively in the past years, the mixed-valence manganate $CaMn_7O_{12}$ distinguishes itself by several prominent features. At low temperatures, the material exhibits a strong magnetoelectric [10,11] and magnetoelastic [12] coupling. The spontaneous ferroelectric polarization saturates at $P_s = 2.9$ mC/m^2 below the temperature of 40 K, which represents the highest value among the currently known magnetically driven ferroelectrics [13]. As a consequence of the magnetoelectric coupling, the polarization decreases in external magnetic field [10]. The spins of the Mn ions are arranged in a way giving rise to a so-called ferroaxial ordering, corresponding to a spiral arrangement of the spins with a chiral symmetry [13]. In different studies, all the three interactions cited above were identified as the dominant coupling mechanism leading to the exceptionally high electric polarization [13–16]. There is no clear agreement about the respective contributions of these mechanisms as yet. Moreover, the record value of P_s for a multiferroic material requires an explanation, which appears to be a challenging task.

The usual way of identifying electromagnons consists in measuring the polarization-sensitive spectra of the infrared (IR) -active excitations polarized along all the crystallographic axes [1,2,17]. In this case, selection rules for the polarization of both the electric and the magnetic vectors of the electromagnetic radiation must be taken into account. Electromagnons can be also distinguished from phonons or purely magnetic active spin waves (magnons) using measurements of the

*Authors to whom correspondence should be addressed: kadlecf@fzu.cz; kamba@fzu.cz

so-called directional dichroism [18–20]. However, both these approaches fail if sufficiently large crystals (thin slabs with two faces of typically several mm^2) are not available. We have shown recently [21] that, in such a case, the electromagnons can be recognized using a combination of unpolarized IR spectra and inelastic neutron scattering (INS). If there are IR-active excitations activated below a magnetic phase transition temperature, which receive dielectric strength from polar phonons, and if these excitations are observed as magnons in the INS spectra, then these excitations can be attributed to electromagnons. In view of this method we have studied, using Fourier-transform IR (FTIR), time-domain THz, and INS spectroscopies, the low-energy spectra of polycrystalline $CaMn_7O_{12}$, in a broad temperature interval from 2 to 590 K.

II. PROPERTIES OF $CaMn_7O_{12}$

At high temperatures, $CaMn_7O_{12}$ has a cubic symmetry with the space group $Im\bar{3}$. The atomic arrangement can be considered [14] as a variant of the perovskite structure with a set of regularly alternating four ABO_3 units and a sum formula $(CaMn_3)Mn_4O_{12}$. This phase features two different Mn positions; one occupying the oxygen octahedra centers with a mixed valence of 3.25, and one placed in the perovskite cube corners, exhibiting a valence of 3 [22]. At $T_{CO} = 440$ K, the compound undergoes a charge-ordering metal-insulator [23] phase transition to a phase with a rhombohedral structure (space group $R\bar{3}$) [24]. In this phase, the mixed-valence Mn atoms shift into two Wyckoff positions—9d and 3b, displaying valences of +3 and +4, respectively; the two kinds of octahedra are subject to two different Jahn-Teller distortions [24].

The next phase transition at $T_{inc} = 250$ K gives rise to Mn orbital ordering [16]. At the same time, an incommensurate structural modulation along the c axis [25] with a propagation vector $q_c \approx (0,0,2.08)$ appears [16]. On further cooling, the crystal undergoes two magnetic phase transitions. At $T_{N1} = 90$ K, a long-range helical antiferromagnetic order with a magnetic superspace group $R31'(00\gamma)ts$ (Ref. [26]) and a spin-induced ferroelectric polarization develop [10,13]; the magnetic propagation vector $q_m = q_c/2$ is temperature independent [12]. The orbital modulation was identified as one of the key elements stabilizing the helical magnetic structure [16]. Below $T_{N2} = 48$ K, a different antiferromagnetic phase is observed, where the magnetic ordering can be described by two temperature-dependent propagation vectors q_{m1} and q_{m2} [13,26]. These are parallel with the c axis, and their average is equal to q_m. Near T_{N2}, a temperature hysteresis of the magnetization was detected [27]. It was shown that the magnetization M below T_{N2} exhibits a memory of the magnetic field applied during the cooldown. The latter observation was interpreted in terms of superparamagnetic clusters, which could be also at the origin of the $M(T)$ hysteresis [27].

III. SAMPLES AND EXPERIMENTAL DETAILS

According to earlier published works, it is very difficult to produce single crystals substantially larger than a fraction of a cubic millimeter [13], which would be necessary for spectroscopic studies with incident waves polarized along the crystallographic axes. Therefore, such studies must be performed on polycrystalline or powder samples only. Our $CaMn_7O_{12}$ powder was prepared by the modified Pechini method using calcium and manganese nitrates in a stoichiometric ratio, ethylene glycol and water. The solution was slowly heated up to 250 °C, the resulting black foam was ground, and the powder was annealed at 830 °C (24 h), 930 °C (48 h), and 950 °C (48 h) with intermittent grinding. Subsequently, the powder was uniaxially pressed at 400 MPa (3 min) to a pellet with a diameter of 12 mm and sintered at 950 °C for 48 h. The density of the pellet was about 80% of the single crystal value. Its phase purity was verified by means of powder x-ray diffraction, excluding other stoichiometry than $CaMn_7O_{12}$ beyond one weight percent. The pellet was thinned down to a thickness of 0.36 mm and optically polished.

IR reflectance and transmittance measurements with a resolution of 2 and 0.5 cm^{-1}, respectively, were performed using the FTIR spectrometer Bruker IFS-113v. An Oxford Instruments Optistat optical cryostat with polyethylene windows was used for sample cooling down to 10 K, and a liquid-He-cooled Si bolometer operating at 1.6 K served as a detector. For measurements at high temperatures, a high-temperature cell (SPECAC P/N 5850) was used. Far-IR transmittance with an applied magnetic field was measured using another Bruker IFS-113v spectrometer and a custom-made cryostat with a superconducting magnet. This setup allowed measurements at 2 and 4 K in the Faraday geometry with an external magnetic field of up to $B_{ext} = 12$ T. Time-domain THz spectroscopy was performed by measuring the complex sample transmittance using custom-made spectrometers based on Ti:sapphire femtosecond lasers; one with an Optistat cryostat, used for measurements without magnetic field, and one with an Oxford Instruments Spectromag cryostat, enabling measurements with $B_{ext} \leqslant 7$ T. Here, the Voigt configuration was used; the electric component of the THz radiation $\mathbf{E}_{THz}$ was set parallel to $\mathbf{B}_{ext}$. Reference measurements with an empty aperture, enabling a reliable determination of the transmittance, were performed systematically at each value of applied magnetic field. The same results, within the experimental accuracy, were obtained also for $\mathbf{B}_{ext} \perp \mathbf{E}_{THz}$.

INS experiments using about 3 g of loose $CaMn_7O_{12}$ powder were performed first at 10 K in the IN4 time-of-flight spectrometer at the Institut Laue-Langevin (ILL Grenoble, France), and within temperatures from 10 to 590 K using the MARI time-of-flight spectrometer at the ISIS facility, Rutherford Appleton Laboratory (UK). The low-temperature dielectric permittivity at 1 kHz was measured in magnetic field of up to 9 T using the high precision capacitance bridge Andeen-Hagerling 2500A in a PPMS 9T instrument, Quantum design.

IV. RESULTS AND DISCUSSION

A. IR spectroscopy

Figure 1 shows the IR reflectivity spectra of $CaMn_7O_{12}$ ceramics at selected temperatures in all known phases. In the high-temperature cubic phase, 13 modes are observed. Moreover, below ca. 150 cm^{-1}, an increase in reflectivity

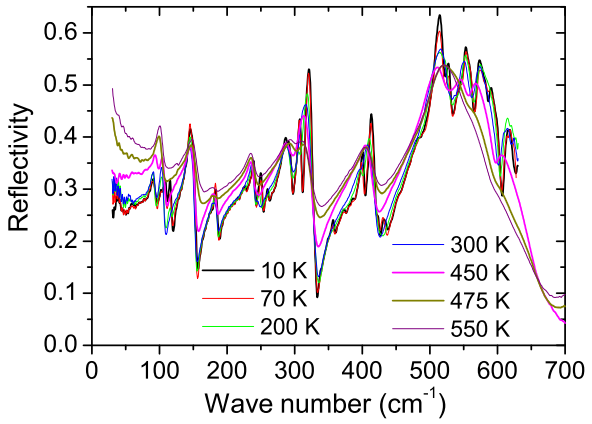

FIG. 1. (Color online) IR reflectivity spectra of $CaMn_7O_{12}$ ceramics in a broad temperature range. The low-temperature spectra above 620 cm^{-1} could not be obtained due to opacity of the polyethylene windows of the cryostat.

towards low frequencies is seen, typical of absorption on free carriers. Below T_{CO}, the sample becomes insulating and the reflection on the free carriers disappears. Upon decreasing temperature and lowering of crystal symmetry, the number of observed polar phonons increases and, at the lowest temperatures, 40 IR-active modes can be distinguished in the reflectivity and transmittance spectra. The frequencies of all observed modes in the whole temperature range are shown in Fig. 2. Here and in the following, ω_j stands for the mode eigenfrequency of the jth mode which can be, in principle, either the transverse optical phonon frequency ω_{TO} or an (electro)magnon frequency ω_{mag}.

We have performed a factor-group analysis of BZ-center lattice vibrations for the cubic $Im\bar{3}$ and trigonal $R\bar{3}$ symmetries. In both crystal structures, the primitive unit cell contains a single formula unit with 20 atoms, implying 60 vibrational degrees of freedom. For the cubic structure, we obtained the following phonon counts:

$$\Gamma_{Im\bar{3}} = 12F_u(\mathrm{IR}) + 2A_u(-) + 2E_u(-) + 2A_g(\mathrm{R}) + 2E_g(\mathrm{R}) + 4F_g(\mathrm{R}), \quad (1)$$

where IR, Raman-active (R), and silent modes (–) are marked in the parentheses. The analysis for the trigonal structure yields

$$\Gamma_{R\bar{3}} = 14E_u(\mathrm{IR}) + 14A_u(\mathrm{IR}) + 6A_g(\mathrm{R}) + 6E_g(\mathrm{R}). \quad (2)$$

Thus, after subtraction of acoustic modes, 11 and 26 IR-active modes are expected in the cubic and trigonal phases, respectively.

The most interesting changes related to the magnetic ordering occur in the frequency range below 80 cm^{-1} (10 meV); they can be well observed in both the FTIR and the THz transmittance spectra. Whereas the FTIR transmittance offers a higher sensitivity especially for photon energies above 7 meV and a better spectral resolution, the measured absorption lines are overlapping with the interference patterns [i.e., the periodic oscillations seen in Fig. 3(a)] arising from multiple reflections of the far-IR waves on the parallel sample surfaces. By contrast, the THz time-domain spectroscopy directly reveals the complex optical constants up to 9 meV, it avoids the

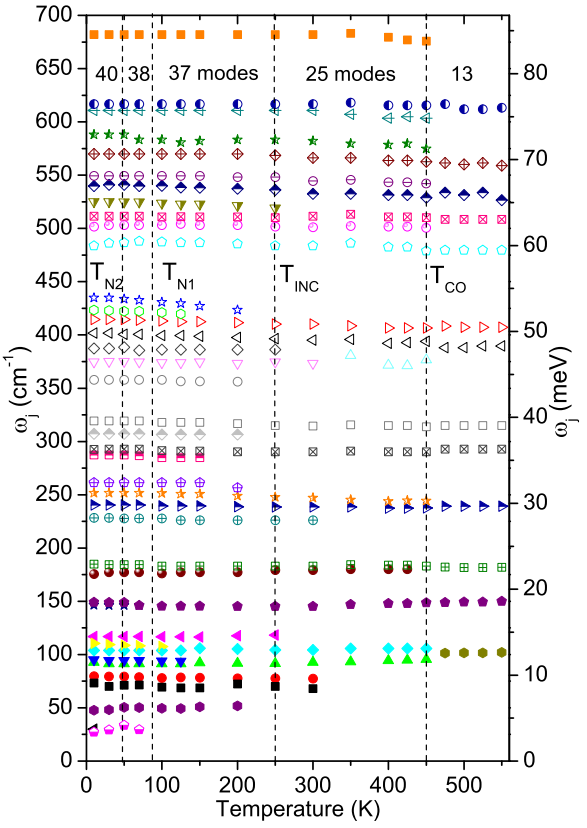

FIG. 2. (Color online) Temperature dependence of the mode eigenfrequencies obtained from fits of IR and THz spectra. The numbers of modes observed in different phases are stated above.

interferences by separating the multiple reflections in time, but it is difficult to achieve a good resolution of narrow spectral lines. Thus, using both these complementary techniques is the best approach for obtaining a detailed spectral information in the far-IR range.

Figure 3(a) shows the far-IR transmittance as a function of temperature. Upon cooling, between 300 and 200 K, the transmittance slightly increases due to a decrease in the phonon damping and the related losses. In contrast, below 200 K, a decrease in the transmittance occurs. At first, a broad absorption band around 50 cm^{-1} gradually develops with cooling, with the fastest increase in its intensity near T_{N1} where the band becomes narrower. Mainly below T_{N2}, another absorption band is seen near 28 cm^{-1}. Analogous changes occur in the spectra of the complex refractive index obtained by THz spectroscopy [see Figs. 3(b) and 3(c)].

Both FTIR transmittance and THz spectra were fitted assuming a sum of Lorentz oscillators describing a dispersion in the dielectric permittivity only. We are keenly aware that this is a rough simplification. Whereas this model is perfectly valid for phonons, i.e., excitations located approximately beyond 90 cm^{-1}, the lower-frequency ones can contribute, to some extent, also to the magnetic permeability. Furthermore, the model of a sum of harmonic Lorentz oscillators is not exact in magnetoelectric multiferroics, since the off-diagonal components of the magnetoelectric susceptibility tensor contribute to the complex index of refraction [19]. Nevertheless, we used

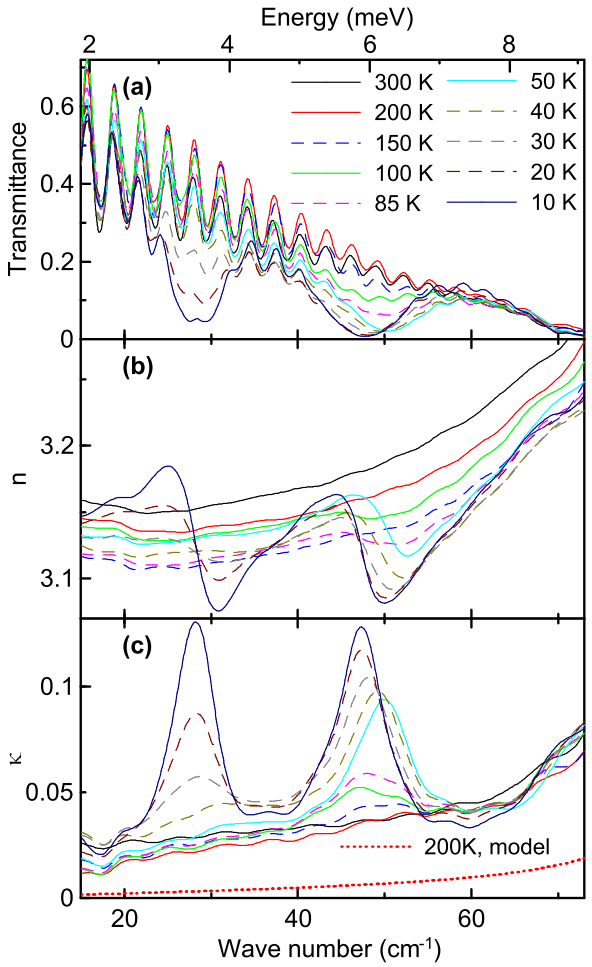

FIG. 3. (Color online) Spectra of (a) far-IR transmittance, (b) real, and (c) imaginary parts of the complex refractive index $N = n + i\kappa$ obtained by THz time-domain spectroscopy. The red dotted line in part (c) shows the low-frequency wing from the phonons at frequencies above 90 cm^{-1}, obtained from fits.

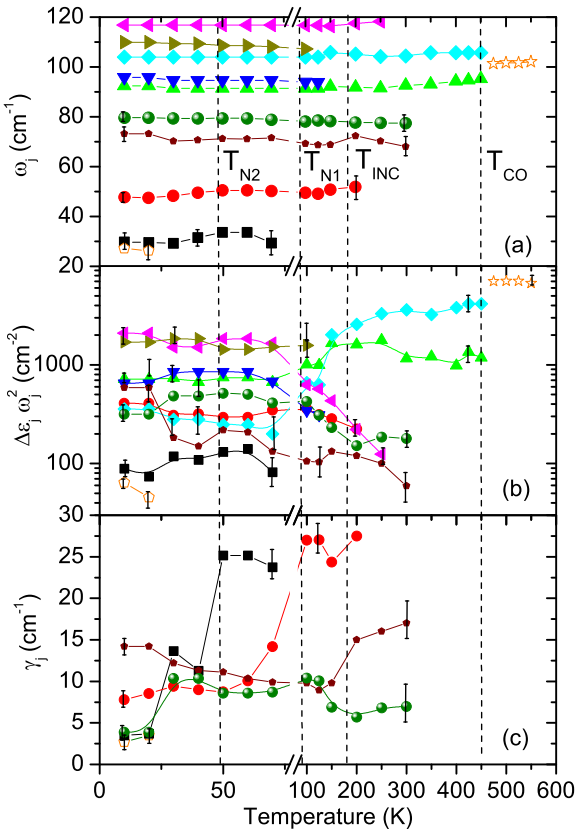

FIG. 4. (Color online) Temperature dependence of (a) frequencies ω_j of the vibrational modes observed below 120 cm^{-1}, (b) their oscillator strengths, and (c) dampings of excitations below 80 cm^{-1}. These parameters were obtained by fitting the measured FTIR and THz spectra. For clarity, the error bars are shown only at selected temperatures. The errors in frequencies of modes above 90 cm^{-1} are smaller than the symbols.

the classical oscillator model to describe the dispersion in N, similar to earlier works (see, e.g., Ref. [2]), which allowed us to determine quantitatively the parameters of all observed excitations.

Careful simultaneous fitting of the IR transmittance, FTIR reflectivity, and THz spectra implies that while there is a single absorption mode near 50 cm^{-1}, the shape of the spectra near 30 and 75 cm^{-1} is such that for their correct modeling, a doublet for each of these regions is required. The temperature dependence of the mode frequencies is shown in Fig. 4(a). The marked anomalies in the intensities (i.e., oscillator strengths $\Delta\varepsilon_j\,\omega_j^2$) and damping constants γ_j of the modes below 60 cm^{-1} near T_{N1} and T_{N2} suggest that these are connected with the magnetic order [see Fig. 4(b)]. Interestingly, the mode seen near 50 cm^{-1} is clearly present with a high damping also in the spectra in the paramagnetic phase at least up to 200 K. As for the doublet near 75 cm^{-1}, the sensitivity of our experimental methods is somewhat lower in this region, but the two modes can be clearly discerned at 10 K. Even at higher temperatures, absorption at these frequencies is necessary for a correct description of the spectra by fitting. As an example, Fig. 3(c) shows a spectrum of the extinction coefficient calculated using a model where only the harmonic oscillators with eigenfrequencies $\omega_j > 90$ cm^{-1} were included; omitting the modes at and below 80 cm^{-1} leads to a marked discrepancy from the experimental data. Thus, thanks to the spectra modeling, we were able to follow these modes between 10 and 300 K. Above room temperature, they may still exist, but the sample becomes opaque in this spectral range, and the modes are probably too weak to be seen in the reflectivity spectra.

Figure 5 shows the spectra of IR transmittance and of the extinction coefficient measured by THz spectroscopy below 80 cm^{-1} at the lowest temperatures, as a function of B_{ext}. The magnetic-field dependence of the mode frequencies is shown in Fig. 6. Two kinds of changes were observed with increasing B_{ext}. First, the frequencies of the modes shift slightly; if a field of $B_{ext} = 7$ T is applied, the modes at 48 cm^{-1} and 28 cm^{-1} harden by about 1 cm^{-1}, whereas the one near 27 cm^{-1} softens by about 1.5 cm^{-1}. Second, additional weaker but clearly observable satellites arise progressively around 55 and 30 cm^{-1} (see Fig. 5). Whereas the position of the satellite near 55 cm^{-1} is independent of the magnetic field, the splitting of the one appearing near 30 cm^{-1} increases up

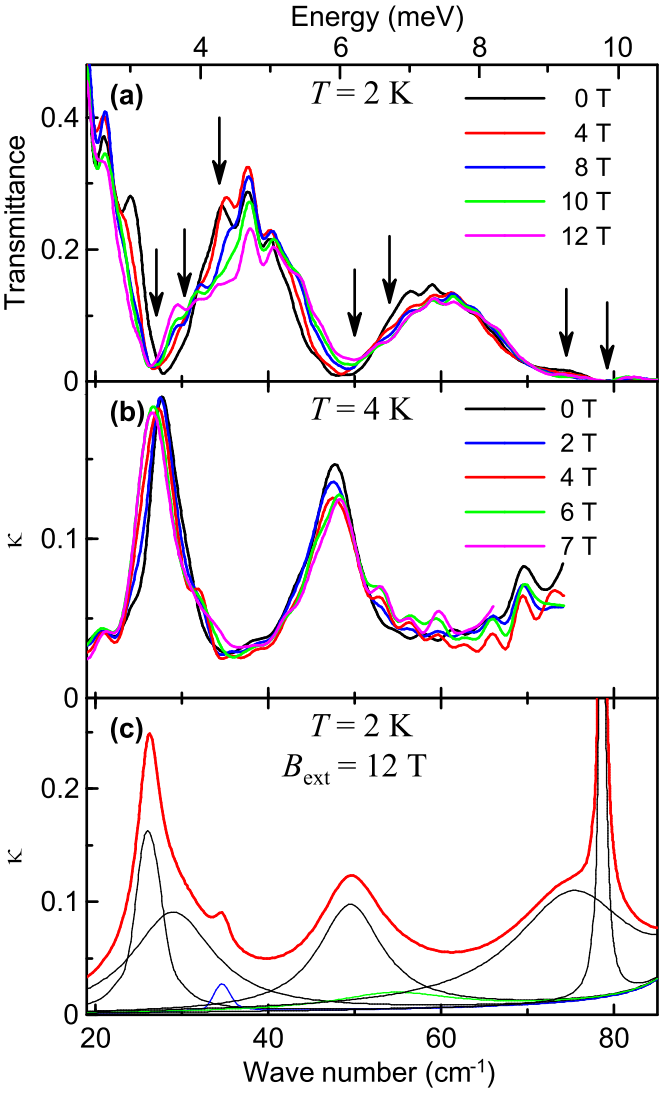

FIG. 5. (Color online) (a) Low-energy FTIR transmittance in external magnetic field (Faraday geometry) at $T = 2$ K. The arrows mark frequencies of modes at $B_{ext} = 12$ T. (b) Extinction coefficient at $T = 4$ K as a function of B_{ext}, obtained by THz spectroscopy in the Voigt geometry. (c) Contributions of individual modes to the extinction coefficient at $T = 4$ K and $B_{ext} = 12$ T, obtained from the fit of the FTIR transmittance.

to ca. 6 cm^{-1} for $B_{ext} = 12$ T. The shapes of the individual lines, contributing to the absorption at this value of B_{ext}, are shown in Fig. 5(c). Such a splitting corresponds qualitatively to a behavior which was theoretically predicted [28] for multiferroics with a spiral arrangement of spins.

The absorption peaks observed for energies below 10 meV can, in principle, be due to phonons or magnons; the changes in the spectra with temperature and magnetic field provide indications for either of these types. The doublet at 75 and 78 cm^{-1} (Fig. 6) is likely due to polar phonons, because it is active already at 300 K. However, one of these modes can be also partly due to a spin excitation, since the magnon density of states (DOS) exhibits a broad maximum in this energy range (see the discussion of the INS data below). In the rhombohedral phase, 25 modes (including these two) are observed, while

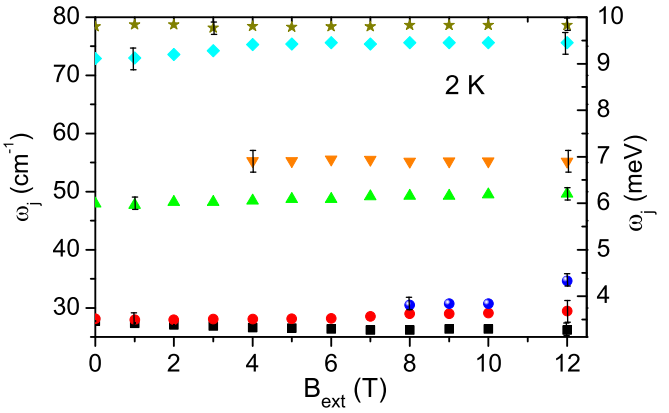

FIG. 6. (Color online) Magnetic-field dependence of the mode frequencies obtained from the spectra fits for $T = 2$ K.

the crystal symmetry allows up to 26 zone-center phonons [see Eq. (2)]. The missing mode can be weak or overlapping with another one. At T_{inc}, $CaMn_7O_{12}$ undergoes a structural phase transition to an incommensurate structure, where 12 new modes appear in the spectra; this kind of transition is known to activate polar phonons due to folding of the BZ [29]. Among them, there are the modes below 60 cm^{-1} which we attribute to spin waves owing to the significant changes in intensities and dampings they exhibit near the magnetic phase transitions and splitting in external magnetic field. Further confirmation of the magnetic character of these modes was obtained by INS.

The oscillator strengths of the excitations below 80 cm^{-1} increase below T_{N1} and T_{N2}, whereas some phonon oscillator strengths decrease below these critical temperatures [see Fig. 4(b)]. Some changes in the oscillator strengths can be caused by mode splitting near 100 K which clearly occurs for phonons above 95 cm^{-1}. At the same time, it is very likely that some strength is also transferred to the newly appearing excitations, which must have a magnetic nature, as discussed below. This would be a signature of dynamic magnetoelectric coupling. Therefore, the observed low-frequency excitations are likely to be electromagnons. A definite confirmation of the electromagnons could be obtained only by an analysis of polarized THz and IR spectra of single crystals, which are currently not available.

B. Inelastic neutron scattering

In a polycrystalline sample, it is not possible to determine directly the phonon and magnon dispersion branches in the BZ. Instead, our data obtained by INS correspond to an orientation-averaged scattering function $S(Q,E)$, where Q is the total momentum transfer and E the energy transferred from the neutrons to the crystal lattice. Beyond the quasielastic neutron scattering (QENS) region, delimited by the energy transfer of $E \approx 1$ meV, three scattering intensity maxima are observed at 10 K for $Q < 1$ Å^{-1} [see Fig. 7(a)]; they occur near $E = 3.5$, 6, and 10 meV, in a very good agreement with the frequencies of the modes observed in IR transmittance and THz spectra (see Fig. 3). It is worth noting that upon heating, this scattering zone becomes broader but it can still be detected

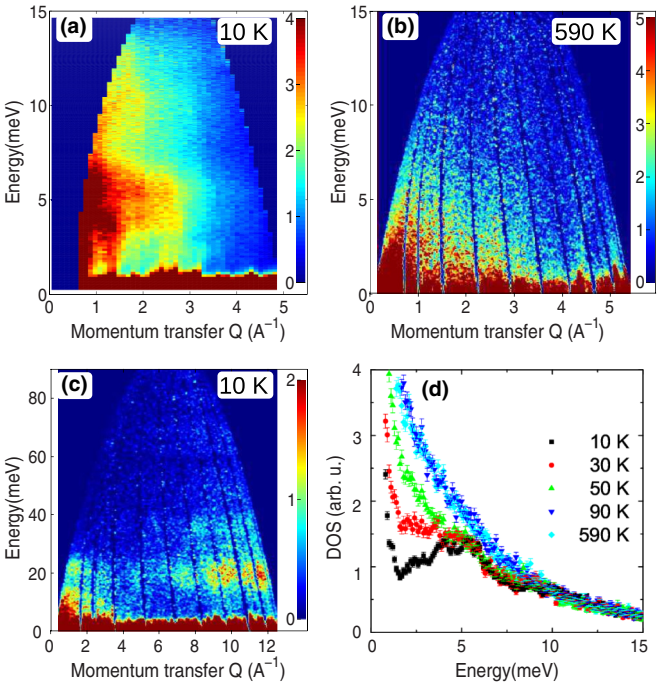

FIG. 7. (Color online) Bose-Einstein-factor-normalized INS intensity at (a) 10 K and (b) 590 K. (c) Map of INS intensity at 10 K in broader Q and E ranges than in (a), showing additionally the phonon absorption at higher Q. Note the different intensity scales in parts (a)–(c). (d) Magnon DOS determined by integrating the INS maps over the Q range from 0.5 to 3 Å^{-1}. The data come from the ISIS facility except the part (a) which was measured in ILL.

up to $T = 590$ K [see Fig. 7(b)]. The magnetic character of these excitations is unambiguously established [30] by the fact that the scattering intensity of magnons decreases with increasing Q. In contrast, the phonons can be observed at higher values of Q; in our case, they were detected at $Q > 7$ Å^{-1} [see Fig. 7(c)]. By integrating $S(Q,E)$ over a low-Q interval for different temperatures, one can obtain the magnon DOS [see Fig. 7(d)]. In general, the peaks in the low-Q DOS correspond to extremes of magnon branches, i.e., to magnons either from the BZ center, BZ boundary, or to a minimum of a magnon branch if the magnetic structure is modulated. It is well known that electromagnons can be activated in the IR spectra just at these wave vectors [6]. Therefore, all the available evidence supports the hypothesis of electromagnon modes in our spectra.

Furthermore, one can see a weaker magnon signal in the INS spectra peaking around 20 meV and $Q < 2$ Å^{-1} [see Fig. 7(c)]. We attribute this signal to two-magnon scattering, which corresponds to the observed maximum in the INS intensity at 10 meV [see Fig. 7(a)]. Alternatively, the weak magnon maximum could be due to one-magnon scattering; one can find also a matching vibrational mode near 20 meV in the IR spectra (Figs. 1 and 2). However, its oscillator strength seems to be too high for a magnon and the shape of the reflectivity spectra does not correspond to a magnon [31]. Therefore, we conclude that the (electro)magnons probably exist up to about 10 meV only.

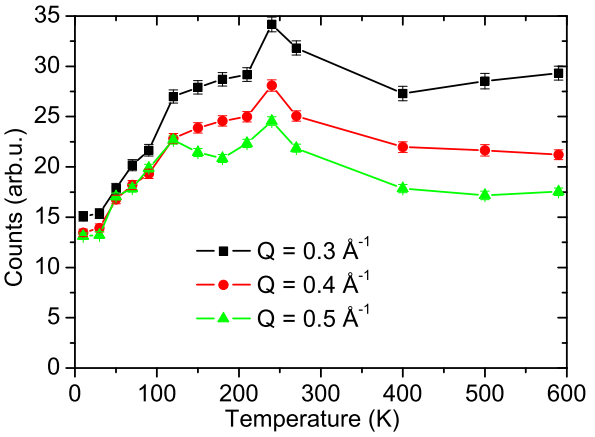

FIG. 8. (Color online) Temperature dependence of the QENS intensity for selected values of Q.

Whereas the existence of the lower-energy magnon band (near 3 meV) in the IR-active spectra is clearly limited to the phase with long-range magnetic ordering which exists below T_{N2}, the mode near 6 meV is strong below T_{N1} but it weakly persists far above T_{N1} (see Fig. 3), as does the magnetic-field sensitive mode near 9 meV. These observations lead us to the conclusion that some kind of short-range magnetic ordering exists even if the long-range magnetic ordering is suppressed by the thermal vibrations. An analogous observation of short-range magnetic order, persisting 15 K above the Néel temperature, was reported recently for nonstoichiometric multiferroic $Ca_{1-x}Cu_xMn_7O_{12}$ [26] with $x \geqslant 0.1$; to our knowledge, no such effect was observed yet for the stoichiometric compound with $x = 0$. We suppose that the absorption maxima near 6 and 9 meV might be linked to short-wavelength (high-wave-vector) magnon modes situated near the BZ boundary and, since these modes are observed throughout the paramagnetic phase, we suggest to call them *paraelectromagnons*. Indications of similar overdamped excitations were observed earlier in paramagnetic phases of other multiferroics, e.g., in $TbMnO_3$ [17], $GdMnO_3$ [32], $TbMn_2O_5$, or YMn_2O_5 [33], but their origin and the reason for their activation in the THz spectra were not discussed in the literature yet. Based on our experimental results, we believe that the paraelectromagnon frequencies correspond to those of magnons from the BZ boundary; their activation would be a consequence of a relaxation in selection rules in the incommensurately modulated magnetic structure. Further, we assume that the paraelectromagnons exist far above T_{N1} due to short-range magnetic correlations and that they are excited by the electric component of the electromagnetic radiation due to magnetostriction, in the same way as zone-boundary electromagnons below T_N [5,6].

The idea of short-range magnetic ordering at temperatures far from the magnetic phase is further supported by our results of the QENS. Figure 8 shows the temperature dependence of the scattering intensity $S(Q,E)$ integrated over the energy interval $0 \leqslant E \leqslant 1$ meV as a function of the momentum transfer Q. Within the whole temperature range (10 to 590 K), a contribution due to coherent QENS was observed with an intensity substantially exceeding the noise floor. Remarkably,

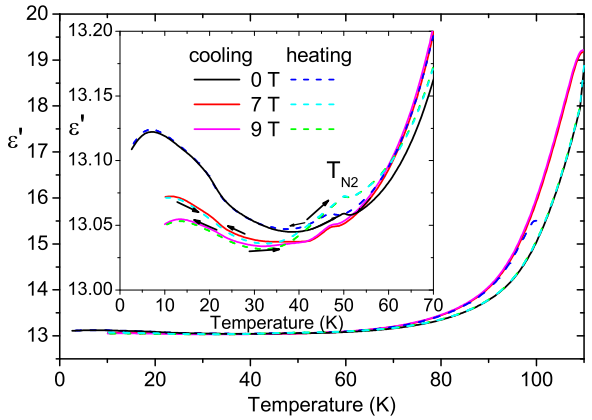

FIG. 9. (Color online) Temperature dependence of the permittivity at 1 kHz upon cooling and heating with various intensities of external magnetic field. The inset shows in detail the temperature region below 70 K.

upon heating above T_{N1}, the QENS intensity increases up to T_{inc} where it reaches the maximum. On further heating, a decrease is observed, but the QENS intensity remains high and approximately constant even in the metallic cubic phase, up to 590 K.

It is worth noting that our observation of presumed electromagnons differs from those reported in single-crystal multiferroics, where a steplike increase in the permittivity often occurs below the temperature where the electromagnon activates [34]. In contrast, for our polycrystalline sample of $CaMn_7O_{12}$, upon cooling, the permittivity decreases substantially down to 40 K due to a drop in conductivity (above 100 K, the loss tangent exceeds unity); we suppose that this compensates the expected increase in the real part of the permittivity upon electromagnon activation. Nevertheless, we observed a small peak in $\varepsilon(T)$ at T_{N2}, followed by an increase below 40 K (see Fig. 9). One can also observe a decrease in permittivity with magnetic field, which can be explained by stiffening of the electromagnons.

V. CONCLUSION

We have performed a thorough spectroscopic study of polycrystalline multiferroic $CaMn_7O_{12}$ over a wide range of temperatures and applied magnetic fields. Our analysis of the FTIR, THz time-domain, and INS spectra proves the existence of magnon modes, including probably one electromagnon at 6 meV and one at 10 meV. In the paramagnetic phase, these modes become heavily damped, largely lose their oscillator strengths, and disappear as much as 100–200 K above T_{N1}. We propose to call such spin modes paraelectromagnons, by analogy with paramagnons. Although our experimental results do not allow us to draw a precise microscopic picture of these modes, the absence of long-range magnetic ordering in the incommensurate phase lets us conclude that the observed absorption peaks near 6 and 10 meV can correspond to dynamical short-range correlations which give rise to a maximum in the magnon DOS at the edge of the BZ. These peaks, together with the unusually strong QENS present up to high temperatures, are apparently linked to the underlying structure and to strong short-range spin-spin interactions, which are also at the origin of the record ferroelectric polarization in $CaMn_7O_{12}$.

Even if our experiments show that the magnetoelectric character of the excitations seen below 10 meV is highly probable, its final confirmation could be obtained only by measurements of directional dichroism or by a detailed polarization analysis of the THz spectra. Unfortunately, such experiments require relatively large single crystals of $CaMn_7O_{12}$, which are currently not available.

ACKNOWLEDGMENTS

This work was supported by the Czech Science Foundation (Project No. P204/12/1163). The kHz-frequency experiments were performed in MLTL (see http://mltl.eu), which is supported within the program of Czech Research Infrastructures (Project No. LM2011025). The experiments in ILL Grenoble were carried out as a part of Project No. LG11024 financed by the Ministry of Education of the Czech Republic.

[1] A. Pimenov, A. M. Shuvaev, A. A. Mukhin, and A. Loidl, J. Phys.: Condens. Matter **20**, 434209 (2008).
[2] N. Kida, Y. Takahashi, J. Lee, R. Shimano, Y. Yamasaki, Y. Kaneko, S. Miyahara, N. Furukawa, T. Arima, and Y. Tokura, J. Opt. Soc. Am. B **26**, A35 (2009).
[3] A. M. Shuvaev, A. A. Mukhin, and A. Pimenov, J. Phys.: Condens. Matter **23**, 113201 (2011).
[4] N. Kida and Y. Tokura, J. Magn. Magn. Mater. **324**, 3512 (2012).
[5] R. Valdés Aguilar, M. Mostovoy, A. B. Sushkov, C. L. Zhang, Y. J. Choi, S.-W. Cheong, and H. D. Drew, Phys. Rev. Lett. **102**, 047203 (2009).
[6] M. P. V. Stenberg and R. de Sousa, Phys. Rev. B **85**, 104412 (2012); **80**, 094419 (2009).
[7] H. Katsura, A. V. Balatsky, and N. Nagaosa, Phys. Rev. Lett. **98**, 027203 (2007).
[8] M. Mochizuki, N. Furukawa, and N. Nagaosa, Phys. Rev. B **84**, 144409 (2011).
[9] S. Seki, N. Kida, S. Kumakura, R. Shimano, and Y. Tokura, Phys. Rev. Lett. **105**, 097207 (2010).
[10] G. Zhang, S. Dong, Z. Yan, Y. Guo, Q. Zhang, S. Yunoki, E. Dagotto, and J.-M. Liu, Phys. Rev. B **84**, 174413 (2011).
[11] M. Sánchez-Andújar, S. Yáñez-Vilar, N. Biskup, S. Castro-García, J. Mira, J. Rivas, and M. Señarís-Rodríguez, J. Magn. Magn. Mater. **321**, 1739 (2009).
[12] W. Sławiński, R. Przeniosło, I. Sosnowska, and M. Bieringer, J. Phys.: Condens. Matter **22**, 186001 (2010).
[13] R. D. Johnson, L. C. Chapon, D. D. Khalyavin, P. Manuel, P. G. Radaelli, and C. Martin, Phys. Rev. Lett. **108**, 067201 (2012).
[14] J. T. Zhang, X. M. Lu, J. Zhou, H. Sun, F. Z. Huang, and J. S. Zhu, Phys. Rev. B **87**, 075127 (2013).
[15] X. Z. Lu, M.-H. Whangbo, S. Dong, X. G. Gong, and H. J. Xiang, Phys. Rev. Lett. **108**, 187204 (2012).
[16] N. Perks, R. Johnson, C. Martin, L. Chapon, and P. Radaelli, Nat. Commun. **3**, 1277 (2012).

[17] Y. Takahashi, N. Kida, Y. Yamasaki, J. Fujioka, T. Arima, R. Shimano, S. Miyahara, M. Mochizuki, N. Furukawa, and Y. Tokura, Phys. Rev. Lett. **101**, 187201 (2008).
[18] I. Kézsmárki, N. Kida, H. Murakawa, S. Bordács, Y. Onose, and Y. Tokura, Phys. Rev. Lett. **106**, 057403 (2011).
[19] I. Kézsmárki, D. Szaller, S. Bordács, V. Kocsis, Y. Tokunaga, Y. Taguchi, H. Murakawa, Y. Tokura, H. Engelkamp, T. Rõõm, and U. Nagel, Nat. Commun. **5**, 3203 (2014).
[20] Y. Takahashi, R. Shimano, Y. Kaneko, H. Murakawa, and Y. Tokura, Nat. Phys. **8**, 121 (2012).
[21] C. Kadlec, F. Kadlec, V. Goian, M. Gich, M. Kempa, S. Rols, M. Savinov, J. Prokleška, M. Orlita, and S. Kamba, Phys. Rev. B **88**, 104301 (2013).
[22] R. Przenioslo, I. Sosnowska, E. Suard, A. Hewat, and A. Fitch, J. Phys.: Condens. Matter **14**, 5747 (2002).
[23] I. O. Troyanchuk, L. S. Lobanovsky, N. V. Kasper, M. Hervieu, A. Maignan, C. Michel, H. Szymczak, and A. Szewczyk, Phys. Rev. B **58**, 14903 (1998).
[24] B. Bochu, J. Buevoz, J. Chenavas, A. Collomb, J. Joubert, and M. Marezio, Solid State Commun. **36**, 133 (1980).
[25] W. Sławiński, R. Przeniosło, I. Sosnowska, and A. Chrobak, J. Phys. Soc. Jpn. **81**, 094708 (2012).
[26] W. Slawinski, R. Przenioslo, I. Sosnowska, and V. Petříček, Acta Crystallogr., Sect. B: Struct. Sci. **68**, 240 (2012).
[27] J. Sannigrahi, S. Chattopadhyay, D. Dutta, S. Giri, and S. Majumdar, J. Phys.: Condens. Matter **25**, 246001 (2013).
[28] H.-B. Chen, Y. Zhou, and Y.-Q. Li, J. Phys.: Condens. Matter **23**, 066002 (2011).
[29] J. Petzelt, Phase Trans. **2**, 155 (1981).
[30] G. Shirane, S. M. Shapiro, and J. M. Tranquada, *Neutron Scattering with a Triple-Axis Spectrometer* (Cambridge University Press, Cambridge, UK, 2002), pp. 36 ff.
[31] A. Mukhin, A. Pronin, A. Prokhorov, G. Kozlov, V. Železný, and J. Petzelt, Phys. Lett. A **153**, 499 (1991).
[32] A. M. Shuvaev, F. Mayr, A. Loidl, A. A. Mukhin, and A. Pimenov, Eur. Phys. J. B **80**, 351 (2011).
[33] A. B. Sushkov, R. V. Aguilar, S. Park, S.-W. Cheong, and H. D. Drew, Phys. Rev. Lett. **98**, 027202 (2007).
[34] A. B. Sushkov, M. Mostovoy, R. V. Aguilar, S.-W. Cheong, and H. D. Drew, J. Phys.: Condens. Matter **20**, 434210 (2008).